Sign reversal of Casimir-Lifshitz torque with separation distance: A theoretical guide to experimentation

Priyadarshini Thiyam ⓘ*

Stranski-Laboratorium für Physikalische and Theoretische Chemie, Institut für Chemie,
Technische Universität Berlin, Strasse des 17. Juni 124, 10623 Berlin, Germany

The Casimir-Lifshitz torque between a pair of birefringent materials was recently shown to exhibit a change in sign with respect to the separation distance owing to the planar dielectric properties of the interacting materials. The recent experiment that verified the existence of the Casimir-Lifshitz torque precluded a sign reversal between the liquid crystal 5CB (4-cyano-4-*n*-pentylbiphenyl) and calcite [Somers *et al.*, Nature (London) **564**, 386 (2018)]. Here, we will show that the sign reversal was not observed in the experiment because it would happen at a larger distance than was investigated for the pairs of materials considered. The purpose of this paper is to identify appropriate choices of combinations of materials that will facilitate experimental observation of the distance-dependent sign reversal of the torque in the experimentally feasible distance regime. Specifically, we propose a setup comprising biaxial black phosphorus and the liquid crystal 5CB or 5PCH (4-cyano-4-*n*-pentylcyclohexane-phenyl) as a particularly viable option. The feature of sign reversal will be an interesting addition to the control mechanism of actuation and switch devices that are applicable for the Casimir-Lifshitz torque.

I. INTRODUCTION

The celebrated Casimir-Lifshitz free energy presented by Dzyaloshinskii, Lifshitz, and Pitaevskii (DLP) predicted that a repulsive force may arise between a pair of interacting materials if $(\varepsilon_1 - \varepsilon_3)$ and $(\varepsilon_2 - \varepsilon_3)$ have opposite signs, where ε_1 and ε_2 are the material permittivities expressed as functions of imaginary frequencies and ε_3 is that of the intervening medium [1]. Since then, a number of studies dealing with repulsive Lifshitz forces have emerged in contexts as varied as nanomechanical engineering [2–4] and environmental systems [5–7]. Such repulsive forces had also already been observed in experiments [8–10]. In an application of the DLP relation taking into account retardation effects, Elbaum and Schick demonstrated that a crossover of the dielectric functions evaluated at imaginary frequencies of ice and water at high frequencies resulted in the formation of water films of finite thickness at the interface [6]. Fundamentally, this means that the interaction energy changes from repulsive to attractive with respect to separation distance. Following this seminal work, various other studies highlighting this important aspect of sign change, with subsequently improved parametrization of the dielectric functions, were explored [11–14]. While such phenomena became widely known in the context of Casimir-Lifshitz interaction energy in three-layer systems, more recently, a similar effect was observed with the Casimir-Lifshitz torque [15].

The Casimir-Lifshitz torque (CLT) between two planar materials arises from the anisotropy of the material polariz-abilities. It induces rotation of the material layers, resulting in alignment of the principal optical axes. The DLP paper mentioned above [1] already predicted it in 1961, and it was recently confirmed experimentally in 2018 [16]. In the perturbative formalism for computing CLT presented in Ref. [15], the expression for torque contains a term, $(\varepsilon_1^{xx} - \varepsilon_1^{yy})(\varepsilon_2^{xx} - \varepsilon_2^{yy})$, resulting from the perturbation parameters. ε_i^{xx} and ε_i^{yy} are the planar components of the dielectric tensors of the interacting materials on the imaginary frequency axis. This term is reminiscent of the DLP relation for a three-layer system. It indicates that a possible change in the direction of the torque may occur if the planar components of one of the interacting materials cross over or intersect at a certain frequency. And, indeed, a sign change with distance was observed between biaxial black phosphorus and rotated P [15]. Subsequently, it was established that, since the term appears under the summation of the Matsubara frequencies, the crossover of the planar components is just a prerequisite but not the deciding factor of the sign reversal [17].

In particular, in the high-precision experiment that established the existence of torque [16], the sign change was not observed in the distance regime probed, that is, within a few tens of nanometers. The experimental measurements were carried out between the liquid crystal 4-cyano-4-*n*-pentylbiphenyl, commonly known as 5CB, and calcite ($CaCO_3$) as the substrate, which possesses intersecting planar dielectric components, thus satisfying the prerequisite of sign change. We will show that theoretical calculations do result in a change in sign of the torque between 5CB and calcite. However, there are several reasons why it was not observed in the experiment; the main reason is that, for this pair of materials, the sign reversal occurs at a separation distance of

*priyadarshini.thiyam@tu-berlin.de

about 822 nm, which is much beyond the distance regime that was investigated in the experiment. We will address the reasons in detail in this work.

In this regard, we demonstrate that biaxial black phosphorus in combination with 5CB will form a suitable pair for uncovering the sign reversal effect in the distance regime feasible for experiments. The choice of P is motivated by its exhibition of in-plane crossing of dielectric functions [15] that suits our purpose. Moreover, bulk P, along with its two-dimensional counterpart, phosphorene, is highly anticipated for potential device applications owing to its desirable material properties such as birefringence [18], variable band gap energies [19,20], and high mobility [21,22], to name a few. Greater torque values were demonstrated with carrier-injected P with excess charge carriers, which also favorably features multiple crossings of the planar dielectric components [17]. However, it is an engineered material which has not been synthesized in the laboratory yet. Here, we consider only original bulk P and focus on the viability of the experimental observation of the sign reversal of the torque.

As for the liquid crystal, 5CB remains our obvious choice since it has already been proven to be accessible in experiments [16]. Additionally, 5CB happens to be one of the few liquid crystals whose refractive index data have been measured experimentally in the desired frequency regime [23]. Frequency-dependent dielectric tensors can be modeled using these data. Since liquid crystals are emerging as good candidates for CLT experiments, we will consider another liquid crystal, 4-cyano-4-n-pentylcyclohexane-phenyl (5PCH), which can also serve as a suitable option for torque measurements. Moreover, studies have shown that liquid crystals display various other interesting Casimir fluctuation phenomena [24,25]. The birefringent property of liquid crystals is exploited in many optoelectronical devices [26,27], which implies a potential for device engineering with CLT as well. CLT is considered to play a vital role in the alignment of liquid crystals and liquid crystal anchoring [28–32].

In the following section, we briefly recapitulate the perturbative theory [15] for CLT used in this work. In Sec. III, we provide the frequency-dependent dielectric functions for the materials considered, and in Sec. IV, we present our results. We make some general remarks on the impact of surface roughness and the possible influence of the free charge carriers of the p-type semiconductor P as well as that of
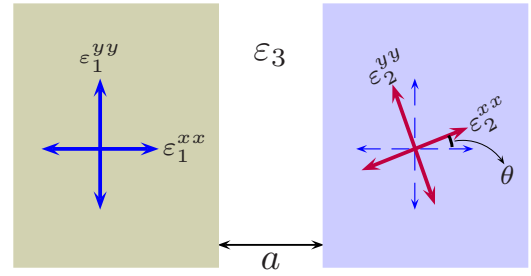

FIG. 1. A pair of dielectric slabs separated by a distance a and an isotropic medium of dielectric function $\varepsilon_3(i\zeta)$. θ is the relative orientation of the principal optical axes of the two slabs. The third principal axis for both the slabs is normal to the plane of the slabs.

electrostatic calibration in the experimental measurements in Sec. V. We end with conclusions in the last section.

II. THEORY

For a pair of planar biaxial materials separated by a distance a as depicted in Fig. 1, the leading-order torque in the perturbative formalism is given by [15,17]

$$\mathcal{T}^{(2)} = -\frac{k_B T \sin 2\theta}{2\pi} \sum_{m=0}^{\infty}{}' \beta_1 \beta_2 \int_0^{\infty} k \, dk \, \text{Tr}(\widetilde{\boldsymbol{R}}_1 \widetilde{\boldsymbol{R}}_2) e^{-2\kappa_3 a}, \quad (1)$$

where k_B is the Boltzmann constant and T is the temperature. The prime on the summation denotes that the zero-frequency mode carries half weight. θ is the angle between the in-plane principal axes of the two slabs, and k is the wave vector perpendicular to the normal of the slabs. $\kappa_3 = \sqrt{k^2 + \zeta_m^2 \varepsilon_3/c^2}$, where $\zeta_m = 2\pi m k_B T / \hbar$ is the imaginary Matsubara frequency $i\zeta$ and ε_3 is the frequency-dependent dielectric function of the intervening isotropic medium. $\beta_i = (\varepsilon_i^{xx} - \varepsilon_i^{yy})/(\varepsilon_i^{xx} + \varepsilon_i^{yy})$ is the perturbative parameter, where ε_i^{xx} and ε_i^{yy} correspond to the planar components of the dielectric functions of the two interacting birefringent materials, while ε_i^{zz} forms the component along the normal direction. The dielectric tensors are taken to be diagonal in this basis of their principal axes. The frequency dependence of the dielectric functions is suppressed for brevity. The reduced reflection coefficients $\widetilde{\boldsymbol{R}}_i$ are given in the Appendix of Ref. [17]. For slabs of infinite thicknesses with an isotropic intervening layer, they take the form

$$\widetilde{\boldsymbol{R}}_i = \begin{bmatrix} \frac{1}{\Delta^H} \frac{\kappa_3 \bar{\kappa}_i^H}{(\kappa_3 + \bar{\kappa}_i^H)^2} & \frac{1}{\sqrt{\Delta^E \Delta^H}} \frac{2\kappa_3 \zeta_m \kappa_i^H}{(\kappa_3 + \bar{\kappa}_i^H)(\kappa_3 + \bar{\kappa}_i^E)} \frac{1}{(\kappa_i^E + \kappa_i^H)} \\ \frac{1}{\sqrt{\Delta^E \Delta^H}} \frac{2\kappa_3 \zeta_m \kappa_i^H}{(\kappa_3 + \bar{\kappa}_i^H)(\kappa_3 + \bar{\kappa}_i^E)} \frac{1}{(\kappa_i^E + \kappa_i^H)} & \frac{1}{\Delta^E} \frac{\kappa_3 \zeta_m^2 \kappa_i^\perp}{\kappa_i^E (\kappa_3 + \kappa_i^E)^2} \end{bmatrix}, \quad (2)$$

where $\Delta^X = (1 - r_{\overline{13}}^X r_{\overline{23}}^X e^{-2\kappa a})$, with $X = E, H$ for the transverse electric (TE) and the transverse magnetic (TM) modes, respectively. $r_{\overline{ij}}^X$ is the reflection coefficient of a uniaxial dielectric slab defined by

$$r_{\overline{ij}}^X = -\frac{\bar{\kappa}_i^X - \bar{\kappa}_j^X}{\bar{\kappa}_i^X + \bar{\kappa}_j^X}, \quad \bar{\kappa}_i^H = \frac{\kappa_i^H}{\varepsilon_i^\perp}, \quad \bar{\kappa}_i^E = \kappa_i^E, \quad (3)$$

where $\kappa_i^H = \sqrt{k^2 \frac{\varepsilon_i^\perp}{\varepsilon_i^{||}} + \frac{\zeta_m^2}{c^2} \varepsilon_i^\perp}$, $\kappa_i^E = \sqrt{k^2 + \frac{\zeta_m^2}{c^2} \varepsilon_i^\perp}$, $\varepsilon_i^\perp = (\varepsilon_i^{xx} + \varepsilon_i^{yy})/2$, and $\varepsilon_i^{||} = \varepsilon_i^{zz}$. For the isotropic intervening layer, $\kappa_3^X = \kappa_3$, and $\bar{\kappa}_3^H = \kappa_3/\varepsilon_3$.

TABLE I. The coefficients of the oscillator dielectric model and the corresponding transition frequencies of the materials considered in this work. *o* and *e* refer to the ordinary and extraordinary components, respectively.

		ω_0 $(10^{14}$ rad/s)	ω_1 $(10^{16}$ rad/s)	ω_2 $(10^{15}$ rad/s)	C_0	C_1	C_2
5CB [23,33]	*o*	66.85	1.567	8.979	0.038	00.414	0.060
	e	66.85	1.567	8.979	0.110	0.459	0.097
5PCH [23]	*o*	80.22	1.396	9.419	0.029	0.387	0.059
	e	80.22	1.396	9.419	0.063	0.456	0.070
Calcite [34,35]	*o*	2.691	1.660		5.300	1.683	
	e	2.691	2.134		6.300	1.182	
Quartz [35]	*o*	2.093	2.040		1.920	1.350	
	e	2.093	2.024		1.960	1.377	
Al$_2$O$_3$ [34]		1.0	2.0		7.03	2.072	
Fused SiO$_2$ [35]		1.880	2.024		1.70	1.098	

III. FREQUENCY-DEPENDENT DIELECTRIC TENSORS

As is obvious from the preceding section, to compute the torque, we require as inputs the dielectric tensors in terms of the imaginary frequencies of the materials involved. The dielectric tensors of 5CB generated using the three-band dispersion model of Wu and coworkers [23] were given in Ref. [33]. Following the same procedure, we model the dielectric functions of 5PCH based on the refractive index data presented in Ref. [23]. In the three-band model of Wu and coworkers, the ordinary (denoted by a subscript *o*) and extraordinary (*e*) refractive indices of a uniaxial liquid crystal are described as [23]

$$n_{(o,e)} = 1 + \sum_{j=0}^{2} g_{j(o,e)} \frac{\lambda^2 \lambda_j^2}{\lambda^2 - \lambda_j^2}, \qquad (4)$$

where $g_{j(o,e)}$ is a proportionality constant comprising the molecular packing density, the number of responsible σ or π electrons, and the oscillator strength. λ_j correspond to the wavelengths at which the three main transitions occur. Equation (4) can be expressed as a function of the imaginary frequencies as

$$\varepsilon_{(o,e)}(i\zeta) = n_{(o,e)}^2(i\zeta) = \left[1 + \sum_{j=0}^{2} \frac{C_{j(o,e)}}{1 + \frac{\zeta^2}{\omega_j^2}} \right]^2, \qquad (5)$$

where $C_{j(o,e)} = g_{j(o,e)} \lambda_j^2$. The values of $g_{j(o,e)}$ and λ_j^2 were given in Ref. [23] and were used in Ref. [33] to calculate and list the values of $C_{j(o,e)}$ for 5CB. Here, we evaluate $C_{j(o,e)}$ for 5PCH and tabulate all the data used in Table I for the convenience of readers. The resulting dielectric tensors are plotted as a function of Matsubara frequencies in Fig. 2 (top left panel). The zero-frequency static values for 5CB are taken from Ref. [33], which provides values of about 18.8 and 6.4 for the extraordinary and ordinary components, respectively, at room temperature. For 5PCH, the values are about $\varepsilon_e(0) \simeq 14$ and $\varepsilon_o(0) \simeq 5$, as provided by Refs. [36–38]. While the refractive indices of many liquid crystals are available in the far-infrared region that can be modeled with Cauchy's fit [39,40], data for the UV region are scarce. The frequency spectrum of the available data is not enough to make plausible

calculations; hence, our choice of liquid crystals considered in this study is limited to 5CB and 5PCH.

The parameters for computing the dielectric functions for uniaxial calcite and crystalline quartz and those of the isotropic materials aluminum oxide (Al$_2$O$_3$) and fused quartz (fused SiO$_2$) are taken from Refs. [34,35]. The Ninham-Parsegian representation for the two-oscillator model is then employed to obtain the dielectric values on the imaginary frequency axis [41,42]:

$$\varepsilon_{(o,e)}(i\zeta) = 1 + \sum_{j=0,1} \frac{C_{j(o,e)}}{1 + \frac{\zeta^2}{\omega_j^2}}. \qquad (6)$$

Equation (5) can be reduced to this familiar form, as done in Ref. [42]. The parameters involved are tabulated together in Table I, and the resulting dielectric functions are plotted in Fig. 2. Note that calcite features a double crossover of its dielectric components, one at a frequency of about 2.8×10^{14} rad/s and the other at about 2.9×10^{16} rad/s (bottom left panel in Fig. 2).

The dielectric tensors of black phosphorus computed using the Vienna Ab initio Simulation Package (VASP) [43–45] within quantum density functional theory were presented in detail in Refs. [15,46]. To briefly summarize the calculation, the revised Heyd-Scuseria-Ernzerhof functional [47,48] was used to determine the optical properties of black P, whose structure was optimized using the Optimized Becke88-van der Waals functional [49,50]. For the relaxation calculation of the structure, the cutoff energy for the plane-wave basis sets was set at 600 eV, while for the optical calculations, it was set at 325 eV. The *k* grids used for the Brillouin zone integration were $8 \times 8 \times 10$. The dielectric components on the imaginary frequency axis were generated using the Kramers-Kronig relation. They are shown in Fig. 2 (top right panel). Note the intersection of the planar *xx* and *yy* components at around 3.89×10^{15} rad/s.

IV. CASIMIR-LIFSHITZ TORQUE

We evaluate the retarded, leading-order contribution to the CLT as given by Eq. (1). Although the perturbative theory presented in Refs. [15,17] takes finite thicknesses explicitly into account, the interacting materials considered here have
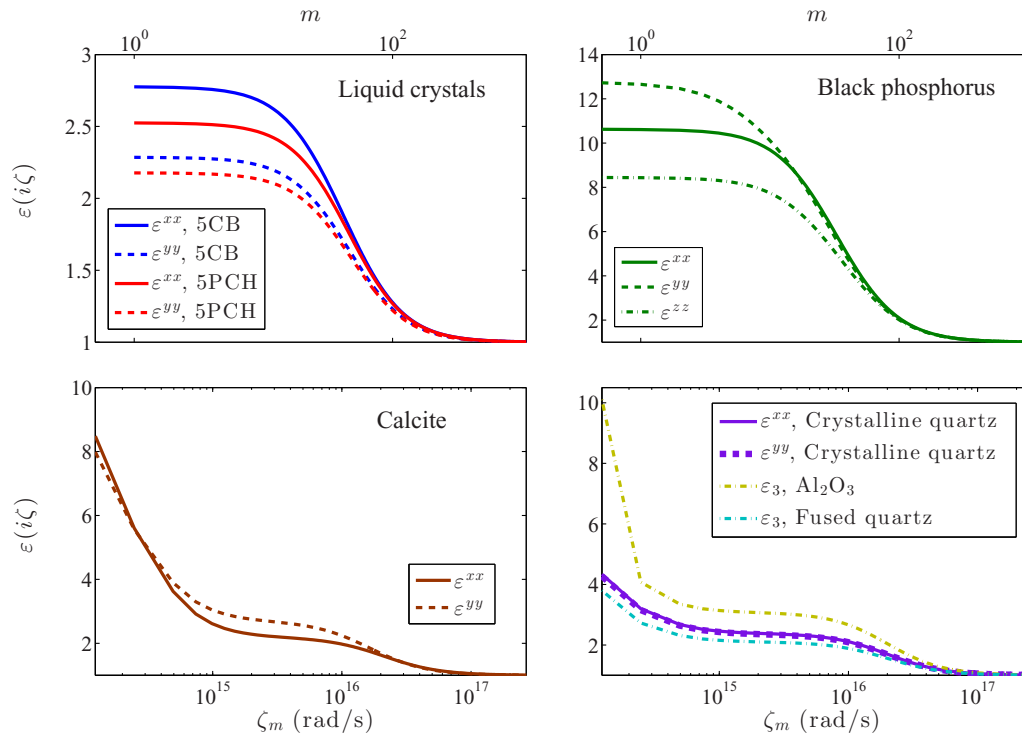
FIG. 2. The components of the dielectric tensors as a function of the Matsubara frequencies for the uniaxial, nematic liquid crystals 5CB [23,33] and 5PCH [23] (top left), calcite [34] (bottom left), crystalline quartz [35] (bottom right), and biaxial bulk black phosphorus [15] (top right). The zero-frequency, static values for 5CB are $\varepsilon^{xx}(0) \simeq 18.8$ and $\varepsilon^{yy}(0) \simeq 6.4$ [33], while those of 5PCH are $\varepsilon^{xx}(0) \simeq 14$ and $\varepsilon^{yy}(0) \simeq 5$ [36–38]. For the rest, the static values are indicated on the y axis. The Matsubara frequency of the bottom x axis corresponds to the Matsubara number m of the top x axis. In our convention, the xx component is taken along the extraordinary axis, and the yy component is taken along the ordinary axis. $\varepsilon^{zz} = \varepsilon^{yy}$ except in the case of biaxial black phosphorus, whose three components are all different. The dielectric functions of the isotropic media Al_2O_3 and fused quartz are also shown in the bottom right panel.

infinite thicknesses. The expression for the torque becomes considerably simpler for infinite slabs, as shown in Sec. II, thus reducing the computation time significantly. This choice is also motivated by the fact that the material thicknesses of about $50\,\mu$m considered by the CLT experiment [16] were shown to be in agreement with Barash's infinite half-space formalism of computing torque for uniaxial materials [51] within the calculation uncertainties. With the perturbative theory, a thickness of $50\,\mu$m results in a difference of about 1% and less in the calculated torque in the relevant distance regime compared with infinitely thick slabs, which is negligible.

We consider the $\pi/4$ orientation of the in-plane principal axes, which produces the maximum value of the torque owing to its $\sin(2\theta)$ dependence. The torque does change sign with respect to θ in general, but here, we will keep θ fixed and study the change in the sign of the torque with respect to the separation distance a. The calculations are done at room temperature ($\sim$298 K).

In Fig. 3, we present the resulting torque between P and 5CB and P and 5PCH separated by the homogeneous, isotropic medium Al_2O_3. The contributions from the TE, TM, and mixed modes are also shown. As expected, the torque reverses sign in both cases and at a distance regime particularly favorable for experimental measurements. The experiment in Ref. [16] measured torque within $\sim$50 nm. Here, the torque between P and 5CB changes sign at about 14 nm, and that

between P and 5PCH changes sign at 17 nm. Although the dielectric modeling of the liquid crystals considered here is not perfect, the behavior of the sign reversal is expected to show up for three reasons: first, the torque is not very sensitive to the dielectric values unlike the Casimir-Lifshitz energies. Second, the sign reversal is a particular attribute of the crossing of the in-plane dielectric functions, which in this case is that of P. The dielectric functions of P were modeled quite accurately [15,46], as there are experimental data available for comparisons [52]. Third, the perturbative calculations of the torque were shown to be very accurate in comparison with Barash's exact result [51] for uniaxial materials with the relative percentage error well below 5% in most cases [15]. The CLT experiment [16] already established good agreement between measured and calculated values using Barash's theory. We anticipate that, with these combinations of materials, the sign reversal effect of the torque with respect to separation distance will manifest itself in experiments.

After the torque changes sign, it exhibits a flat peak of the order of $\sim 2.4 \times 10^{-10}$ J/m^2 in magnitude for both cases which then gradually goes to zero with separation distance. It is clear from the contribution curves of the individual modes in Fig. 3 that the sign change is mostly brought about by the TM mode. The mixed mode tends to have a larger magnitude than the TE mode.

To determine the robustness of the sign reversal effect, we carry out the same calculations with these pairs of materials
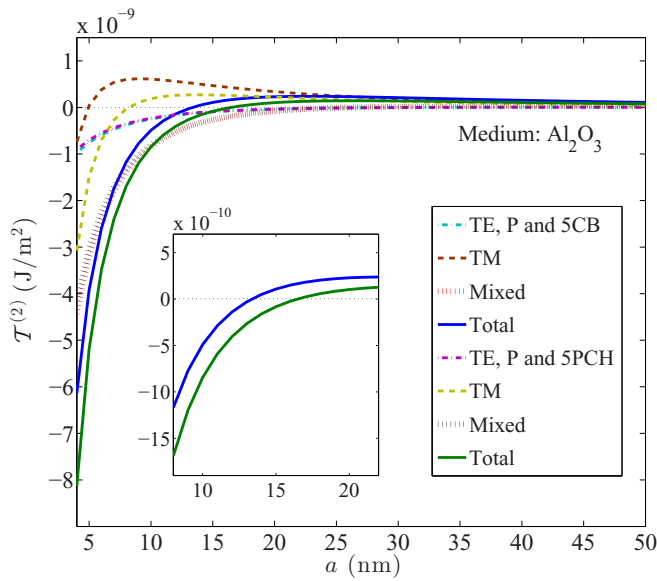
FIG. 3. Torque per unit area as a function of separation distance between P and 5CB and P and 5PCH with an intervening homogeneous layer of Al_2O_3. The contributions from the TE, TM, and mixed modes are also indicated. The inset highlights the sign reversal of the torque with respect to distance for both cases.

FIG. 5. Torque per unit area as a function of separation distance between P and 5CB and P and 5PCH with vacuum in between the interacting slabs. The contributions from the TE, TM, and mixed modes are also indicated. The inset highlights the sign reversal of the torque with respect to distance for both cases.

but with the intervening medium being fused quartz and vacuum, although the latter setup is probably not supported by experiments yet. The first case is shown in Fig. 4. With fused quartz as the isotropic material filling the gap between P and the liquid crystals, the sign change occurs at 18 nm in the case of 5CB and at 21 nm in the case of 5PCH. With vacuum as the separating medium, the torque between P and 5CB changes
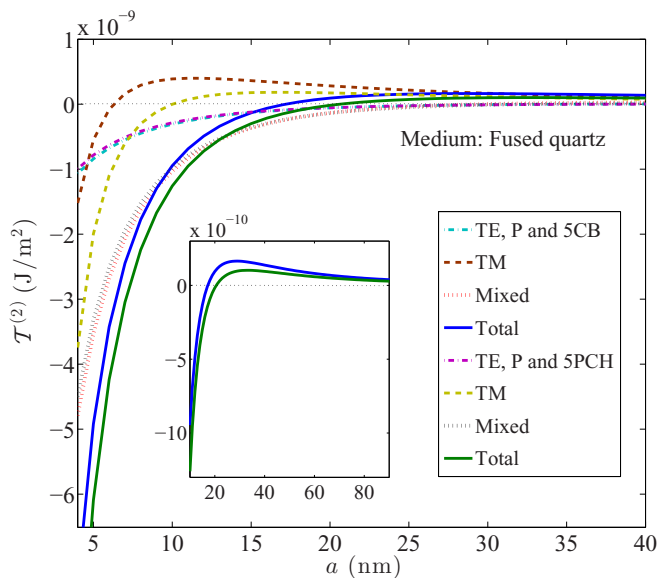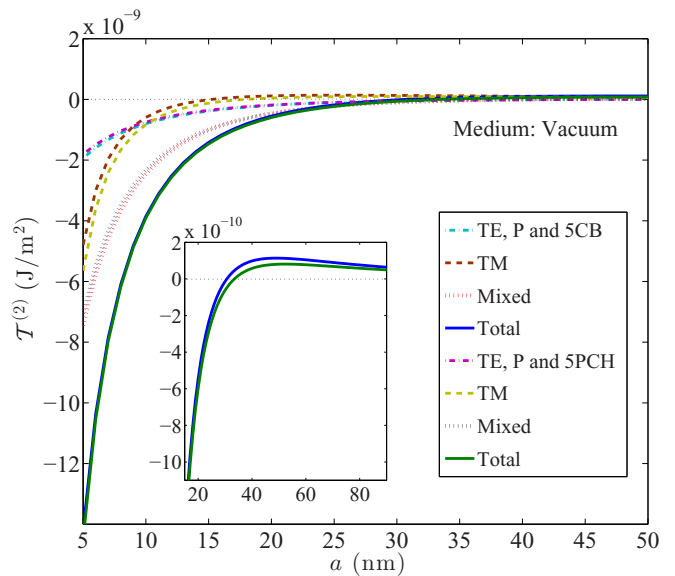

FIG. 4. Torque per unit area as a function of separation distance between P and 5CB and P and 5PCH with an intervening homogeneous layer of fused quartz. The contributions from the TE, TM, and mixed modes are also indicated. The inset highlights the sign reversal of the torque with respect to distance for both cases.

sign at 31 nm, and that between P and 5PCH changes sign at 34 nm, as demonstrated in Fig. 5. The distances at which the reversal of the sign of the torque occurs conveniently fall within the experimental regime. The contributions of the modes show a trend similar to the one seen before. An interesting observation is that the medium induces faster reversal of the sign of torque, that is, at smaller separation distance than for vacuum. This seems to indicate that the sign reversal is a property of the optical length of the medium. That is, the longer physical length of the vacuum and the shorter physical length of the medium may be playing a role in determining the corresponding distances of sign reversal. This matter will be further investigated in detail in future work.

To address the issue of nonobservance of the sign reversal of torque in the CLT experiment [16], we calculate the torque between 5CB and calcite with the intervening medium Al_2O_3 and plot it as a function of separation distance in Fig. 6. This setup corresponds exactly to that considered by the experiment. The sign change does occur, but at a distance of 822 nm. This regime of very large separation distances was not probed by the experiment. In addition, the magnitude of the torque is too small at this distance to result in any probable physical change in the system that could be detected by experiments. The torque between 5PCH and calcite separated by Al_2O_3 changes sign at 824 nm.

In the right panel of Fig. 6, we also plot the torque between calcite and the liquid crystals with fused quartz as the intervening medium. The sign change consistently appears for these pairs, but at a distance of 794 nm for both cases, which is again not going to be very useful for experiments. It is interesting how switching the liquid crystals hardly affects the distance at which the torque changes direction. This prompted us to perform the torque calculations for calcite and another uniaxial material, crystalline quartz, in the three different
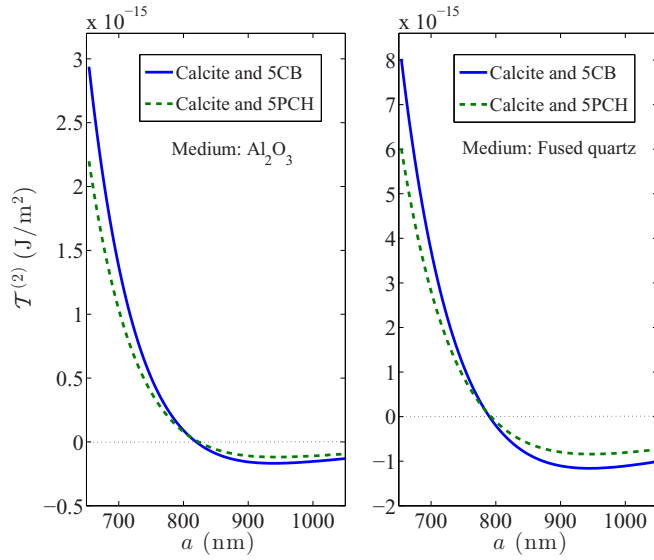
FIG. 6. Torque per unit area as a function of separation distance between $CaCO_3$ and 5CB and $CaCO_3$ and 5PCH with an intervening layer of Al_2O_3 (left panel) and fused SiO_2 (right panel), highlighting the distance regime at which the sign of the torque reverses.

TABLE II. The estimated (Est.) distance a_c, predicted empirically, and the observed (Obs.) distance a_c, determined theoretically, for all the configurations considered in this work.

Medium	First slab	Second slab	a_c (nm)	
			Obs.	Est.
Al_2O_3	P	5CB	14	24
	P	5PCH	17	24
	P	Quartz	18	24
	Calcite	5CB	822	268
	Calcite	5PCH	824	268
	Calcite	Quartz	776	268
Fused SiO_2	P	5CB	18	19
	P	5PCH	21	19
	P	Quartz	22	19
	Calcite	5CB	794	326
	Calcite	5PCH	794	326
	Calcite	Quartz	756	326
Vacuum	P	5CB	31	39
	P	5PCH	34	39
	P	Quartz	39	39
	Calcite	5CB	1088	536
	Calcite	5PCH	980	536
	Calcite	Quartz	1324	536

media. The result is shown in Fig. 7. The torque reverses sign at 776, 756, and 1324 nm for Al_2O_3, fused SiO_2, and vacuum, respectively.

In this regard, a theoretical estimation of the form $a_c = c/(2\zeta_c\sqrt{\varepsilon_m(\zeta_c)})$ was presented in Refs. [7,15] following Ref. [53], wherein the frequency ζ_c at which the in-plane dielectric components intersect dictates at what distance a_c the sign change will occur roughly. This gives, for the case of calcite-quartz, approximately 268, 326, and 536 nm for the media Al_2O_3, fused quartz, and vacuum, respectively, corresponding to an intersection frequency of 2.8×10^{14} rad/s. Note that a second intersection frequency, 2.9×10^{16} rad/s, of calcite does not result in any sign change at very short

separation distances. Although the estimation correctly predicts the order of magnitude for a_c, it is obvious that the dielectric components of the other material without planar crossing do play a role as well. In the case of calcite, the underestimation of a_c seems more prominent. Nevertheless, the qualitative prediction serves as a good tool in the initial scanning of the sign reversal of the torque without having to perform the computation for a wide range of separation distances. The theoretically predicted and empirically estimated distances of sign reversal for the pairs of materials and media considered are tabulated in Table II.

Finally, we consider the combination of P and crystalline quartz in order to highlight P, with the in-plane dielectric components crossing at $\zeta_c = 3.89 \times 10^{15}$ rad/s, as a very suitable material that induces sign reversal at appropriate, experimentally feasible distances. The resulting torque is plotted in Fig. 8, with the sign reversal occurring at 18, 22, and 39 nm for the intervening media Al_2O_3, fused SiO_2, and vacuum, respectively. The empirical estimation seems to work better for black P than for calcite (see Table II). Again, the presence of a medium between the interacting materials brings about the sign reversal faster.

The question of sign reversal does not arise if the materials involved do not feature any crossings in their planar dielectric functions. Figure 9 gives an example to illustrate just that. The substrate considered here is crystalline quartz paired with 5CB and 5PCH. The torque is scanned over a wide range of distance regimes plotted in log scale in Fig. 9. We also tested other substrates such as $BaTiO_3$ and BeO with noncrossing planar dielectric functions [34,54] to verify the nonappearance of the sign change in such cases (results not shown). This result is, however, routine. The presence of a medium is known to induce a greater magnitude of torque rather than
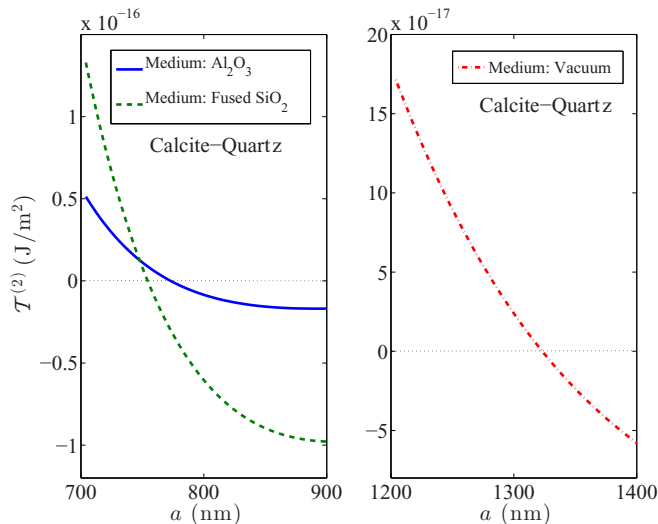

FIG. 7. Torque per unit area as a function of distance between calcite and crystalline quartz separated by different intervening isotropic layers.
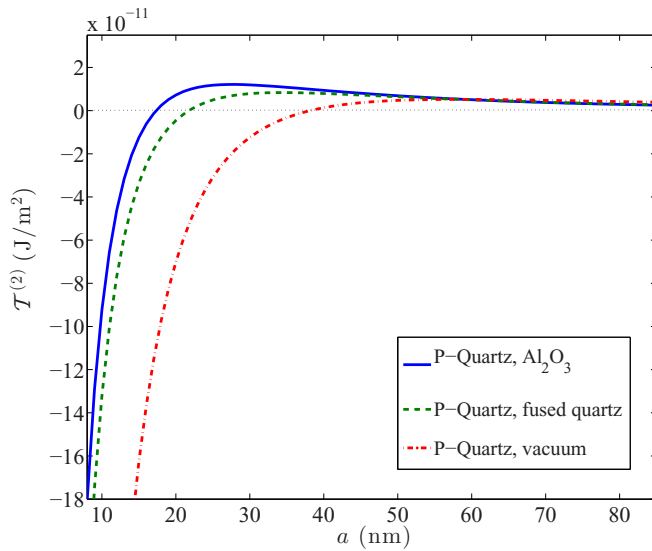
FIG. 8. Torque per unit area as a function of separation distance between black phosphorus and crystalline quartz with the three different intervening layers.

FIG. 10. Torque per unit area as a function of separation distance between pairs of liquid crystals. The inset highlights the curves below 40 nm.

screening the interaction [54,55] and has been attributed to the complex nature of the interaction involving retardation, anisotropy, and orientation angles of the interacting materials. For the quartz–liquid crystal system considered here, neither Al_2O_3 nor fused SiO_2 results in a greater magnitude of the torque than in vacuum, as is evident in Fig. 9.

Now, in the simple three-layer system comprising a pair of liquid crystals, we do not expect the torque to change sign since none of them has any in-plane crossing of the dielectric functions, which is confirmed in Fig. 10. However, Broer *et al.* recently observed a sign change with respect to distance in the torque between cholesteric liquid crystals modeled as planar multilayer stacks [56]. The cholesteric liquid crystal considered in their study comprised 96% nematic 5CB and 4% chiral
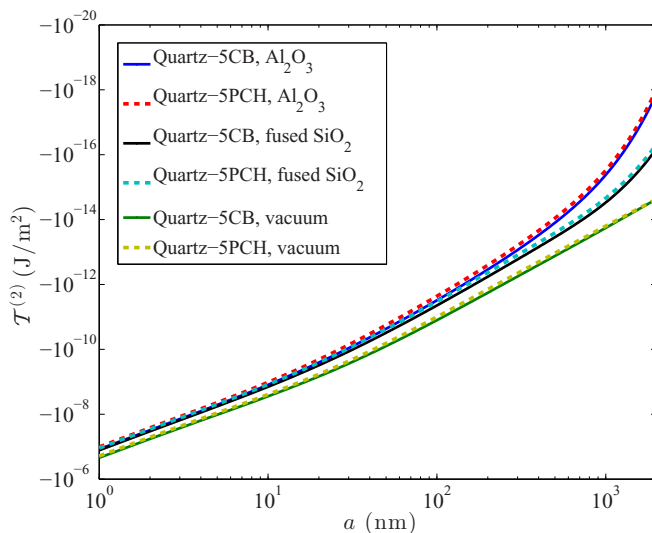

FIG. 9. Torque per unit area as a function of separation distance between crystalline quartz and the liquid crystals in the presence of different isotropic layers.
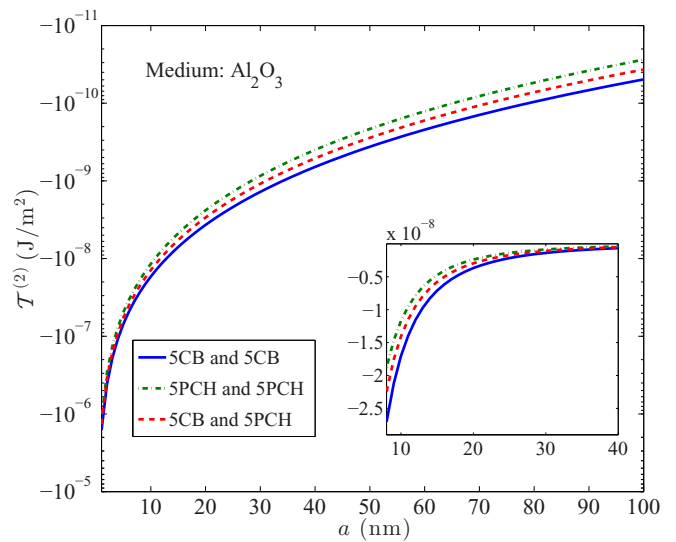
dopant by mass. It is remarkable that the sign reversal with distance can also occur due to the interplay of the dielectric functions in multilayer structures.

V. SOME GENERAL REMARKS ON THE EFFECT OF SURFACE ROUGHNESS, ELECTROSTATIC CALIBRATION, AND FREE CHARGE CARRIERS

In the nanometer regime of separation distances, the effect of surface roughness will be non-negligible [57–59]. In the CLT experiment in Ref. [16], the intervening isotropic layer (Al_2O_3) was directly deposited on the birefringent substrate, while an isotropic surfactant layer (FC-4430) was inserted between the liquid crystal and the open side of the Al_2O_3 layer facing the liquid crystal to avoid the liquid crystal sticking at the interfaces. The surface roughness was determined to be about 4–5 nm, and the extent of the surfactant layer was determined to be about ∼8 nm [16]. Even with the distance offset of 12 nm employed in the experiment, it should be possible to observe the sign reversal effect of the CLT for some of the pairs of materials considered in this paper. It was further found that the presence of FC-4430 has little effect on the torque [16].

In cases involving calcite where sign reversal occurs at separations of the order of 1 μm, an alternative experimental technique involving electrostatic calibration [60] may be more suitable for the determination of absolute separation distances and calibration parameters.

Bulk black P, being an intrinsic *p*-type semiconductor, possesses some electrical conductivity and resistivity [61]. In this regard, an effect of excess charge carriers was studied in Ref. [17], which found that carrier concentration of the order of 10^{19}/cm^3 and above was required to bring about a significant change in the dielectric tensors from that of the original bulk P and the resulting torque. Thus, the few charge carriers that may be present in the original bulk P will not affect the torque. Although small concentrations of free charge carriers

have been known to alter the Casimir energies and the forces [62], that is not so much the case with torque (at least for bulk P).

VI. CONCLUSIONS

Using a reliable perturbative theory [15,17], this work demonstrated that a configuration comprising a common liquid crystal, 5CB, paired with naturally occurring biaxial black phosphorus will lead to a sign reversal of the Casimir-Lifshitz torque with a separation distance in the regime accessible by experiments. Another liquid crystal, 5PCH, was shown to exhibit similar behavior and offers an alternative choice. As for the substrate, very few naturally available uniaxial or biaxial materials feature an in-plane crossing of their planar dielectric components, which is a prerequisite to the sign reversal of

the torque in three-layer systems. The substrate calcite does possess the necessary requirements, but it steers the sign reversal towards very large separation distances unsuitable for experimental observation. Nevertheless, many engineered materials are under study which could effectuate the sign reversal behavior. Experimental confirmation of the stated effect would not only validate the theoretical predictions and set forth further investigations but would also expedite practical, nanotechnological applications.

[1] I. E. Dzyaloshinskii, E. M. Lifshitz, and L. P. Pitaevskii, General theory of van der Waals' forces, Sov. Phys. Usp. **4**, 153 (1961).

[2] U. Leonhardt and T. G. Philbin, Quantum levitation by left-handed metamaterials, New J. Phys. **9**, 254 (2007).

[3] A. A. Feiler, L. Bergström, and M. W. Rutland, Superlubricity using repulsive van der Waals forces, Langmuir **24**, 2274 (2008).

[4] F. Capasso, J. N. Munday, D. Iannuzzi, and H. B. Chan, Casimir forces and quantum electrodynamics torques: Physics and nanomechanics, IEEE J. Sel. Top. Quantum Electron. **13**, 400 (2007).

[5] S. Lee and W. M. Sigmund, Repulsive van der Waals forces for silica and alumina, J. Colloid Interface Sci. **243**, 365 (2001).

[6] M. Elbaum and M. Schick, Application of the Theory of Dispersion Forces to the Surface Melting of Ice, Phys. Rev. Lett. **66**, 1713 (1991).

[7] M. Boström, O. I. Malyi, P. Parashar, K. V. Shajesh, P. Thiyam, K. A. Milton, C. Persson, D. F. Parsons, and I. Brevik, Lifshitz interaction can promote ice growth at water-silica interfaces, Phys. Rev. B **95**, 155422 (2017).

[8] E. S. Sabisky and C. H. Anderson, Verification of the Lifshitz theory of the van der Waals potential using liquid-helium films, Phys. Rev. A **7**, 790 (1973).

[9] J. N. Munday, F. Capasso, and V. A. Parsegian, Measured long-range repulsive Casimir-Lifshitz forces, Nature (London) **457**, 170 (2009).

[10] R. Zhao, L. Li, S. Yang, W. Bao, Y. Xia, P. Ashby, Y. Wang, and X. Zhang, Stable Casimir equilibria and quantum trapping, Science **364**, 984 (2019).

[11] J. Fiedler, M. Boström, C. Persson, I. H. Brevik, R. W. Corkery, S. Y. Buhmann, and D. F. Parsons, Full-spectrum high resolution modeling of the dielectric function of water, J. Phys. Chem. B **124**, 3103 (2020).

[12] M. Boström, V. Esteso, J. Fiedler, I. Brevik, S. Y. Buhmann, C. Persson, S. Carretero-Palacios, D. F. Parsons, and R. W. Corkery, Self-preserving ice layers on CO_2 clathrate particles: Implications for Enceladus, Pluto and similar ocean worlds, Astron. Astrophys. **650**, A54 (2021).

[13] J. Luengo-Márquez and L. G. MacDowell, Lifshitz theory of wetting films at three phase coexistence: The case of ice nucleation on silver iodide (AgI), J. Colloid Interface Sci. **590**, 527 (2021).

[14] Y. Li, K. A. Milton, I. H. Brevik, O. I. Malyi, P. Thiyam, C. Persson, D. F. Parsons, and M. Boström, Premelting and formation of ice due to Casimir-Lifshitz interactions: Impact of improved parameterization for materials, Phys. Rev. B **105**, 014203 (2022).

[15] P. Thiyam, P. Parashar, K. V. Shajesh, O. I. Malyi, M. Boström, K. A. Milton, I. Brevik, and C. Persson, Distance-Dependent Sign Reversal in the Casimir-Lifshitz Torque, Phys. Rev. Lett. **120**, 131601 (2018).

[16] D. A. T. Somers, J. L. Garett, K. J. Palm, and J. N. Munday, Measurement of the Casimir torque, Nature (London) **564**, 386 (2018).

[17] P. Thiyam, P. Parashar, K. V. Shajesh, O. I. Malyi, M. Boström, K. A. Milton, I. Brevik, and J. Forsman, Effect of excess charge carriers and fluid medium on the magnitude and sign of the Casimir-Lifshitz torque, Phys. Rev. B **100**, 205403 (2019).

[18] L. Shulenburger, A. D. Baczewski, Z. Zhu, J. Guan, and D. Tománek, The nature of the interlayer interaction in bulk and few-layer phosphorus, Nano Lett. **15**, 8170 (2015).

[19] L. Li, J. Kim, C. Jin, G. J. Ye, D. Y. Qiu, F. H. da Jornada, Z. Shi, L. Chen, Z. Zhang, F. Yang, K. Watanabe, T. Taniguchi, W. Ren, S. G. Louie, X. H. Chen, Y. Zhang, and F. Wang, Direct observation of the layer-dependent electronic structure in phosphorene, Nat. Nanotechnol. **12**, 21 (2017).

[20] Y. Maruyama, S. Suzuki, K. Kobayashi, and S. Tanuma, Synthesis and some properties of black phosphorus single crystals, Physica B+C (Amsterdam) **105**, 99 (1981).

[21] J. Qiao, X. Kong, Z.-X. Hu, F. Yang, and W. Ji, High-mobility transport anisotropy and linear dichroism in few-layer black phosphorus, Nat. Commun. **5**, 4475 (2014).

[22] X. Wang, A. M. Jones, K. L. Seyler, V. Trans, Y. Jia, H. Zhao, H. Wang, L. Yang, X. Xu, and F. Xia, Highly anisotropic and robust excitons in monolayer black phosphorus, Nat. Nanotechnol. **10**, 517 (2015).

[23] S.-T. Wu, C.-S. Wu, M. Warenghem, and M. Ismaili, Refractive index dispersions of liquid crystals, Opt. Eng. **32**, 1775 (1993).

[24] F. K. P. Haddadan, A. Naji, A. K. Seifi, and R. Podgornik, Pseudo-Casimir interactions across nematic films with disor-

dered anchoring axis, J. Phys.: Condens. Matter **26**, 075103 (2014).

[25] F. K. P. Haddadan, A. Naji, and R. Podgornik, Casimir-like interactions and surface anchoring duality in bookshelf geometry of smectic-A liquid crystals, Soft Matter **15**, 2216 (2019).

[26] S. T. Wu and D. K. Yang, *Reflective Liquid Crystal Displays* (Wiley, New York, 2001).

[27] A. R. Khokhlov and A. V. Emelyanenko, Nanostructured liquid crystal systems and applications, Beilstein J. Nanotechnol. **9**, 2644 (2018).

[28] E. R. Smith and B. W. Ninham, Response of nematic liquid crystals to van der Waals forces, Physica (Amsterdam) **66**, 111 (1973).

[29] E. Dubois-Violette and P. G. De Gennes, Effects of long range van der Waals forces on the anchoring of a nematic fluid at an interface, J. Colloid Interface Sci. **57**, 403 (1976).

[30] M. Schadt, K. Schmitt, V. Kozinkov, and V. Chigrinov, Surface-induced parallel alignment of liquid crystals by linearly polymerized photopolymers, Jpn. J. Appl. Phys. **31**, 2155 (1992).

[31] G. P. Bryan-Brown, E. L. Wood, and I. C. Sage, Weak surface anchoring of liquid crystals, Nature (London) **399**, 338 (1999).

[32] M. Lu, Liquid crystal orientation induced by van der Waals interaction, Jpn. J. Appl. Phys. **43**, 8156 (2004).

[33] P. E. Kornilovitch, van der Waals interaction in uniaxial anisotropic media, J. Phys.: Condens. Matter **25**, 035102 (2013); Corrigendum: Van der Waals interaction in uniaxial anisotropic media (2013 J. Phys.: Condens. Matter **25**, 035102), **30**, 189501 (2018).

[34] L. Bergström, Hamaker constants of inorganic materials, Adv. Colloid Interface Sci. **70**, 125 (1997).

[35] D. B. Hough and L. R. White, The calculation of Hamaker constants from Lifshitz theory with applications to wetting phenomena, Adv. Colloid Interface Sci. **14**, 3 (1980).

[36] B. Gestblom and S. Urban, Dielectric relaxation studies of 5PCH by the time domain spectroscopy method, Z. Naturforsch **50**, 595 (1995).

[37] J. Kumar, R. K. Gupta, S. Kumar, and Manjuladevi V., Electro-optic and dielectric studies on quantum dot doped nematic liquid crystal, Macromol. Symp. **357**, 47 (2015).

[38] Shivaraja S. J., R. K. Gupta, S. Kumar, and Manjuladevi V., Effect of functionalised silver nanoparticle on the elastic constants and ionic transport of a nematic liquid crystal, Liq. Cryst. **46**, 1868 (2019).

[39] J. Li and S.-T. Wu, Extended Cauchy equations for the refractive indices of liquid crystals, J. Appl. Phys. **95**, 896 (2004).

[40] J. Li, C.-H. Wen, S. Gauza, R. Lu, and S.-T. Wu, Refractive indices of liquid crystals for display applications, J. Display Technol. **1**, 51 (2005).

[41] J. Mahanty and B. W. Ninham, *Dispersion Forces* (Academic, London, 1976).

[42] D. A. T. Somers and J. M. Munday, Rotation of a liquid crystal by the Casimir torque, Phys. Rev. A **91**, 032520 (2015).

[43] G. Kresse and J. Hafner, *Ab initio* molecular dynamics for liquid metals, Phys. Rev. B **47**, 558 (1993).

[44] P. E. Blöchl, Projector augmented-wave method, Phys. Rev. B **50**, 17953 (1994).

[45] G. Kresse and D. Joubert, From ultrasoft pseudopotentials to the projector augmented-wave method, Phys. Rev. B **59**, 1758 (1999).

[46] P. Thiyam, A study of finite-size, non-perturbative and anisotropic effects on the Lifshitz-van der Waals forces and torque with material dielectric responses from first-principles calculations, Ph.D. thesis, KTH Royal Institute of Technology, 2018.

[47] J. Heyd, G. E. Scuseria, and M. Ernzerhof, Hybrid functionals based on a screened Coulomb potential, J. Chem. Phys. **118**, 8207 (2003).

[48] A. V. Krukau, O. A. Vydrov, A. F. Izmaylov, and G. E. Scuseria, Influence of the exchange screening parameter on the performance of screened hybrid functionals, J. Chem. Phys. **125**, 224106 (2006).

[49] J. Klimeš, D. R. Bowler, and A. Michaelides, Chemical accuracy for the van der Waals density functional, J. Phys.: Condens. Matter **22**, 022201 (2010).

[50] J. Klimeš, D. R. Bowler, and A. Michaelides, Van der Waals density functionals applied to solids, Phys. Rev. B **83**, 195131 (2011).

[51] Y. S. Barash, Moment of van der Waals forces between anisotropic bodies, Izv. Vyssh. Uchebn. Zaved., Radiofiz. **21**, 1637 (1978) [Radiophys. Quantum Electron. **21**, 1138 (1978)].

[52] T. Nagahama, M. Kobayashi, Y. Akahama, S. Endo, and S. Narita, Optical determination of dielectric constant in black phosphorus, J. Phys. Soc. Jpn. **54**, 2096 (1985).

[53] B. W. Ninham and V. A. Parsegian, Biophys. J. **10**, 646 (1970).

[54] J. N. Munday, D. Iannuzzi, Y. Barash, and F. Capasso, Torque on birefringent plates induced by quantum fluctuations, Phys. Rev. A **71**, 042102 (2005).

[55] D. A. T. Somers and J. N. Munday, Casimir-Lifshitz Torque Enhancement by Retardation and Intervening Dielectrics, Phys. Rev. Lett. **119**, 183001 (2017).

[56] W. Broer, B.-S. Lu, and R. Podgornik, Qualitative chirality effects on the Casimir-Lifshitz torque with liquid crystals, Phys. Rev. Res. **3**, 033238 (2021).

[57] M. Bordag, G. L. Klimchitskaya, and V. M. Mostepanenko, The Casimir force between plates with small deviations from plane parallel geometry, Int. J. Mod. Phys. A **10**, 2661 (1995).

[58] P. A. Maia Neto, A. Lambrecht, and S. Reynaud, Casimir effect with rough metallic mirrors, Phys. Rev. A **72**, 012115 (2005).

[59] W. Broer, G. Palasantzas, J. Knoester, and V. B. Svetovoy, Roughness correction to the Casimir force at short separations: Contact distance and extreme value statistics, Phys. Rev. B **85**, 155410 (2012).

[60] C.-C. Chang, A. A. Banishev, R. Castillo-Garza, G. L. Klimchitskaya, V. M. Mostepanenko, and U. Mohideen, Gradient of the Casimir force between Au surfaces of a sphere and a plate measured using an atomic force microscopy in a frequency-shift technique, Phys. Rev. B **85**, 165443 (2012).

[61] Y. Zhang, J. Wang, Q. Liu, S. Gu, Z. Sun, P. K. Chu, and X. Yu, APL Mater. **8**, 120903 (2020).

[62] G. L. Klimchitskaya, U. Mohideen, and V. M. Mostepanenko, The Casimir force between real materials: Experiment and theory, Rev. Mod. Phys. **81**, 1827 (2009).